Chemical and Process Engineering 2014, 35 (2), 191-204
DOI: 10.2478/cpe-2014-0015

BED-TO-WALL HEAT TRANSFER IN A SUPERCRITICAL CIRCULATING FLUIDISED BED BOILER

Artur Błaszczuk*[1], Wojciech Nowak[1], Szymon Jagodzik[2]

[1]Częstochowa University of Technology, Institute of Advanced Energy Technologies, Dabrowskiego 73, 42-200 Częstochowa, Poland

[2]Tauron Generation S.A., Łagisza Power Plant, Pokoju 14, 42-504 Będzin, Poland

The purpose of this work is to find a correlation for heat transfer to walls in a 1296 t/h supercritical circulating fluidised bed (CFB) boiler. The effect of bed-to-wall heat transfer coefficient in a long active heat transfer surface was discussed, excluding the radiation component. Experiments for four different unit loads (i.e. 100% MCR, 80% MCR, 60% MCR and 40% MCR) were conducted at a constant excess air ratio and high level of bed pressure (ca. 6 kPa) in each test run. The empirical correlation of the heat transfer coefficient in a large-scale CFB boiler was mainly determined by two key operating parameters, suspension density and bed temperature. Furthermore, data processing was used in order to develop empirical correlation ranges between 3.05 to 5.35 $m \cdot s^{-1}$ for gas superficial velocity, 0.25 to 0.51 for the ratio of the secondary to the primary air, 1028 to 1137K for bed temperature inside the furnace chamber of a commercial CFB boiler, and 1.20 to 553 $kg \cdot m^{-3}$ for suspension density. The suspension density was specified on the base of pressure measurements inside the boiler's combustion chamber using pressure sensors. Pressure measurements were collected at the measuring ports situated on the front wall of the combustion chamber. The obtained correlation of the heat transfer coefficient is in agreement with the data obtained from typical industrial CFB boilers.

Keywords: heat transfer coefficient, suspension density, furnace temperature, circulating fluidised bed, supercritical CFB boiler, cluster renewal approach

1. INTRODUCTION

The circulating fluidised bed (CFB) technology is the combustion technology most widely used for heat and power generation using solid fuels including biomass (Kobyłecki, 2011). In the last 20 years a rapid development of the technology of fuel combustion in a circulating fluidised bed has been observed, resulting in progressively increasing the size of units. Since the capacity of commercial CFB boilers increases, the study on the heat transfer coefficient at water-wall surface in contact with fluidised mass is highly required to design and scale-up heat transfer surface inside the furnace. Properly designed heat transfer surfaces inside a combustion chamber allow controlling and maintaining the optimum operating temperature. Major heat transfer surfaces are located above the secondary air injection in the combustion chamber of CFB boilers. In the upper part of furnace chamber, water-wall surfaces absorb roughly 40%-60% of heat released from combustion products (Basu and Cheng, 2000). At furnace corners in large size CFB boilers, heat transfer is slightly smaller than that on the vertical water-wall. Moreover, heat transfer data from 135 MWe CFB unit indicated

*Corresponding author, e-mail: ablaszczuk@is.pcz.czest.pl

that the heat transfer coefficient at the furnace corners was 6%-8% higher than that on the vertical membrane-wall (Zhang et al., 2005).

Heat transfer to walls of a circulating fluidised bed furnace is dependent on the bed hydrodynamic conditions. In CFB boilers, solid suspension density (Breitholz et al., 2001; Cheng et al., 2007) and furnace temperature (Błaszczuk et al., 2012) are dominant parameters exerting the strongest influence on the heat transfer coefficient. Many experimental investigations in large-scale CFB combustors aimed at determination of heat transfer to the vertical water-wall surface furnace have been published (Cheng et al., 2007; Dutta and Basu, 2002; Koksal et al., 2008; Nirmal and Reddy, 2005). In Table 1 the heat transfer coefficient formulas correlated with suspension density using regression analysis are given. In industrial CFB boilers, collecting information on suspension density is not accessible during boiler operation. Interestingly though, the pressure drop along height of furnace chamber is usually measured. Based on the pressure distribution inside a combustion chamber, the average suspension density can be estimated.

Moreover, heat transferred from fluidised medium to the membrane water-walls of circulating fluidised bed boiler depends on the particle diameter of bed material (suspension) and the solid circulation rate. Many investigations on the effects of the bed particle size on heat transfer in the circulating fluidised bed are available in the published literature (Andersson, 1996; Gungor, 2009; Pagliuso et al., 2000). Some works studied the effect of solids circulation rate on the bed to membrane wall heat transfer coefficient (Feugier et al., 1987; Tiany and Peng, 2004; Xie et al., 2003).

Table 1. Summary of empirical correlations of heat transfer coefficient in large-scale CFB boilers (Gorliz and Grace, 2002)

Researcher	Empirical correlation	Solid suspension density in furnace ρ_b [kg·m^{-3}]	Temperature in furnace T_b [K]
Andersson and Leckner (1992)	$h = 30\ (\rho_b)^{0.5}$	5-80	1023-1168
Gorliz and Sunden (1994)	$h = 88 + 9.45\ (\rho_b)^{0.5}$	7-70	1073-1123
Basu and Nag (1994)	$h = 40\ (\rho_b)^{0.5}$	5-20	1023-1123
Andersson (1996)	$h = 70\ (\rho_b)^{0.085}$ $h = 58\ (\rho_b)^{0.36}$	>2 ≤2	910-1156

The relationship between the heat transfer coefficient and the particle diameter or solids circulation rate was described in detail by Shi et al. (1998) and Xie et al. (2003), respectively and will not be repeated in this work.

This work reports and analyses the experimental results obtained from an operating supercritical CFB boiler for the average bed to membrane water wall heat transfer coefficient. A mechanistic model based on cluster renewal approach was used to predict the bed-to-wall heat transfer coefficient in a 1296 t/h supercritical CFB boiler. The research includes a study on the effects of average suspension density. An empirical correlation of the heat transfer coefficient was proposed for a large-scale supercritical CFB boiler.

2. CLUSTER RENEWAL MODEL OF HEAT TRANSFER

In the present model the hydrodynamic parameters of the circulating fluidised bed system were taken into account. In CFB boilers the gas-solid flow pattern above the refractory line (i.e. the secondary air injection level) inside the furnace chamber is typically of a core-annulus structure. In the core with a dilute suspension, solids move upward with an occasional presence of clusters. The gas velocity in the

dilute core is well above the superficial gas velocity, while that in the annulus is low to negative, because solids in form of clusters move downwards. The downward velocity of clusters in the annulus region is between 2 and 8 $m \cdot s^{-1}$ in large-scale CFB boilers (Werther, 2005). In a certain distance from the membrane wall, outside the thin gas layer, particles form clusters and then solid agglomerates disintegrate as shown in Fig. 1. The gas gap thickness δ between the wall and the cluster is calculated using an expression given by Lints et al. (1994).

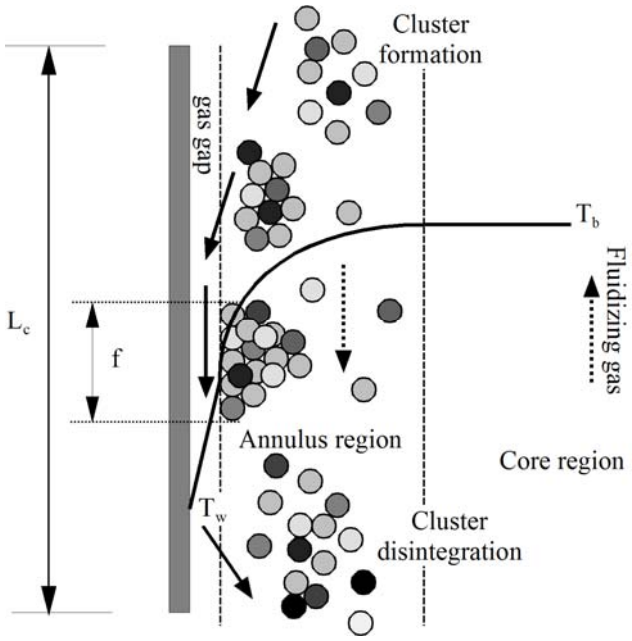

Fig. 1. Conceptual view of cluster and gas gap close to a membrane-wall (Nirmal Vijay et al., 2005)

Based on these considerations, the membrane wall comes interchangeably in contact with clusters and the dispersed phase. The cluster characteristic travel length L_c and residence time t_c (i.e. time of contact between cluster and the wall) depend upon bed hydrodynamic conditions and they can be estimated in a CFB unit from Eq. (1) proposed by Wu et al. (1991) and Eq. (2) given by Noymer et al. (2000), respectively.

$$L_c = 0.0178\rho_b^{0.596} \tag{1}$$

$$t_c = \frac{L_c}{U_c} = \frac{L_c}{0.75 \cdot \left(\rho_p g d_p / \rho_g\right)^{0.5}} \tag{2}$$

In this mechanistic model, the heat transfer coefficient between the membrane wall and the bed includes contributions of particle convection h_p, gas convection h_g, cluster convection h_c, gas conduction h_w and radiation h_{rad}. The radiation heat transfer coefficient is a combination of radiation from the clusters h_{rc} and from the dispersed phase h_{rd}. Thus, in circulating fluidised bed combustors the overall bed-to-wall heat transfer coefficient above the secondary air injection level in dilute phase is given by Eq. (3):

$$h = h_{conv} + h_{rad} = fh_p + (1-f)h_g + fh_{rc} + (1-f)h_{rd} \tag{3}$$

where f denotes the fractional wall coverage by clusters and is calculated using the expression (4) given by Duta et al. (2004):

$$f = 1 - exp\left(-4300\{1-\varepsilon\}^{1.39}\{D_h/H\}^{0.22}\right) \tag{4}$$

The derivation of the coefficients in Eq. (4) was estimated on basis of data from several commercial CFB boilers. The heat transfer equations (5)-(8) used in this mechanistic model are given in Table 2

and formulas needed for estimating the physical and thermal properties of cluster and also typical flue gas of a coal-fired fluidised bed can be found in (Basu, 2006).

Table 2. *Heat transfer equations used in the model*

$h_p = \frac{1}{\left(\frac{1}{h_c}+\frac{1}{h_w}\right)} = \frac{1}{\left(\frac{\pi t_c}{4k_c\rho_c c_c}\right)^{0.5} + \frac{d_p\delta}{k_g}}$ (5)	$h_{rc} = \frac{\sigma\cdot\left(T_b^4 - T_w^4\right)}{\left(1/e_c + 1/e_w - 1\right)\cdot\left(T_b - T_w\right)}$ (7)
$h_g = \frac{k_g c_p}{d_p c_g}\cdot\left(\frac{\rho_d}{\rho_p}\right)^{0.3}\cdot\left(\frac{U_t^2}{g d_p}\right)^{0.21}\cdot \mathrm{Pr}$ (6)	$h_{rd} = \frac{\sigma\cdot\left(T_b^4 - T_w^4\right)}{\left(1/e_d + 1/e_w - 1\right)\cdot\left(T_b - T_w\right)}$ (8)

The relations for the dispersed phase density ρ_d, emissivity of the cluster e_c and emissivity of the dispersed phase e_d can be found in Nirmal Vijay et al. (2005).

3. DESCRIPTION OF SUPERCRITICAL CFB BOILER

A performance test on a 1296 t/h supercritical CFB boiler was carried out jointly by Czestochowa University of Technology and Tauron Generation, including the measurements of pressure and temperature within the combustion chamber. Unlike typical CFB boilers this boiler is equipped with a vertically tubed BENSON evaporator**,** which is a new supercritical steam technology. The supercritical steam generation technology was described in detail elsewhere (Goidich, 2007). This CFB steam generator contains furnace, solids separators, INTREX^{TM} integrated heat exchangers (Fig. 2a.) and a low-temperature flue-gas heat recovery system. The supercritical CFB boiler has a power of 966 MW_{th} and a height of 48.0 m. The cross-sectional area is 27.6×10.6 m^2 in the transport zone where the heat transfer surfaces in the form of membrane water-walls are located. In the bottom part up to 9.0 m height, the walls are covered with refractory lining. A fluidisation grid with nozzles of primary air is situated at the bottom of combustion chamber (Fig. 2b). Secondary air nozzles are located at three levels above the grid.

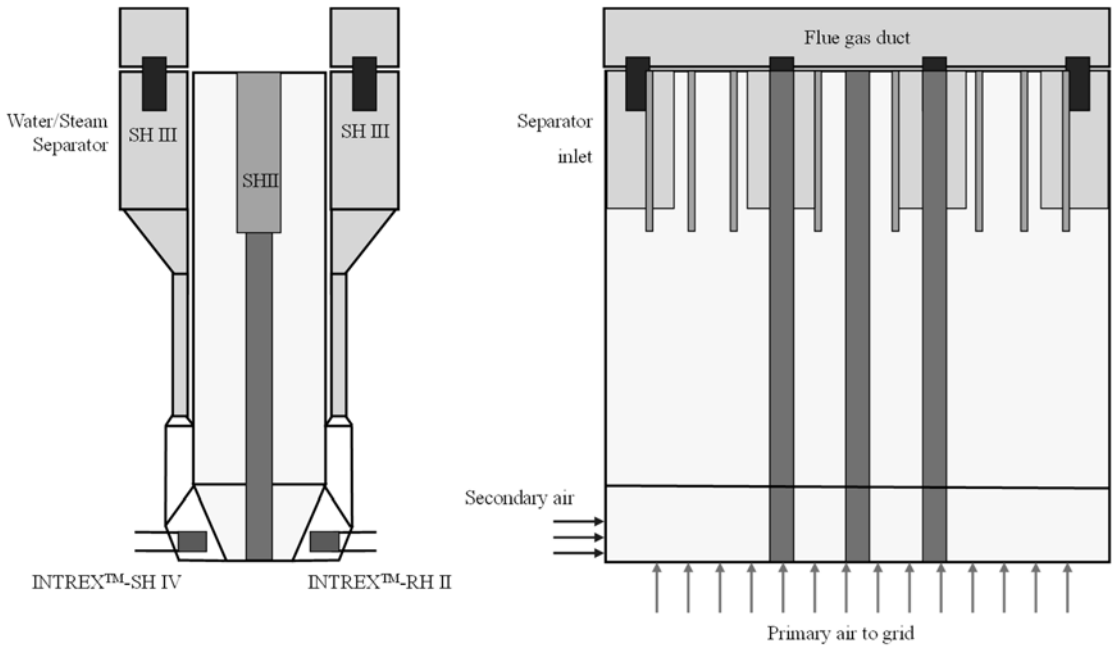

Fig. 2. Schematic layout of utility supercritical CFB boiler;
a) arrangement of superheaters (SH) and reheater (RH); b) arrangement of air distribution

The boiler is equipped with 8 compact separators of loose material, which are located in 4 along both sidewalls. The separators are made of membrane walls, which are covered with a thin layer of erosion-resistant refractory. A similar construction characterises solids particles' return leg to the chamber of the fluidized bed heat exchangers (INTREX^{TM}), which are integrated with boiler's sidewalls. The construction of the INTREX^{TM} chamber has a wall seal structure. In the INTREX^{TM} chambers the heat is transferred with circulating material to the superheater and reheater tube bundles immersed in a fluidised bed.

4. EXPERIMENTAL CONDITIONS

The complete list of temperature and pressure measurement points is given in Table. 3. When stable operating conditions in the CFB combustor had been achieved, three measurement series were conducted. The measurements of pressure along the height of combustion chamber were taken between 0.2 m and 42.4 m above the primary air distributor level. Because of a foreseen high vertical pressure gradient of the bed material at the bottom part of combustion chamber, the measurement ports were densely spaced in this area. The temperature inside the furnace chamber was measured by 11 thermocouples of type K with ± 0.1°C accuracy, in direct contact with the gas-solid suspension flow. Temperature measurements were collected in 8 measuring ports located between 0.25 m and 42.4 m from the fluidisation grid. The thermocouples signals were transferred via an A/D converter to a hard disk of PC for recording. DASYLab software was used to archive measured results during all test runs. The sampling interval of signals was selected at 100 kHz. Temperature signals were collected during sampling time of 5s for each test run. The local measurement data from the large-scale supercritical CFB boiler are presented as 30 sec averages. Both pressure and temperature data were measured in the centre-line of the front wall, because the variation across the wall is small, being approximately ±0.05 kPa and ±280.3 K for pressure and temperature respectively. Therefore, it was assumed that the centre-line values are representative for the height where they were collected.

Table 3. Levels of measurement ports in the furnace chamber of the supercritical CFB boiler

Temperature measurement ports	Pressure measurement ports	Furnace height from air distributor, H [m]
√	√	0.25
n/a	√	0.4
n/a	√	0.6
√	√	1
√	√	2
n/a	√	2.5
√	√	5
√	√	8.3
√	√	24
√	√	31
√	√	42.4

The average suspension density was calculated from measured static pressure drops along the height of furnace chamber using the following equation:

$$\rho_b = 9.81^{-1}\left(P_i - P_{i+1}\right)\left(H_i - H_{i+1}\right)^{-1} \tag{9}$$

where H_i and H_{i+1} denote the measurement positions closest to the upper and lower end of wall, respectively, and P_i and P_{i+1} are the corresponding pressures. Attrition and gas-particle acceleration effects were neglected in Eq. (9).

Performance tests were carried out during a four day period with each test run lasting six hours. Before each test run, the operation conditions of the boiler (Table 4) were let to stabilise for four hours. One measurement series was generally run for ca. 2 hours.

Table 4. Operating range of the 1296 t/h CFB boiler during the tests

Operating parameter	Unit	Range of variation
Superficial gas velocity, U_o	$m \cdot s^{-1}$	3.05-5.35
Terminal velocity, U_t	$m \cdot s^{-1}$	1.30-1.61
Minimum fluidisation velocity, U_{mf}	$m \cdot s^{-1}$	0.00723-0.00770
Ratio of secondary air to the primary air, *SA/PA*	-	0.25-0.51
Pressure drop, Δp	kPa	5.76-7.26
Furnace temperature, T_b	K	1033-1153
Suspension density, ρ_b	$kg \cdot m^{-3}$	1.2-553

All tests were conducted at a high level of bed pressure, p_{bed}, which was in the range from 5.4 kPa to 6.8 kPa, and at different levels of boiler loads (i.e. 100% MCR, 80% MCR 60% MCR and 40% MCR), maintaining a constant excess air ratio in each test run. The fuel used in the experiments is a Polish bituminous coal and the proximate and ultimate analysis data are given in Table 5 and Table 6, respectively.

Table 5. Approximate analysis of bituminous coal used in performance tests

Specification		Unit	Test #1	Test #2	Test #3	Test #4
LHV	Q^{ar}	MJ/kg	23.87	22.08	21.73	22.92
Ash	A^{ar}	wt %	9.70	12.87	10.82	10.38
Moisture	W^{ar}	wt %	13.38	11.93	13.82	14.37
- free		wt %	10.20	8.43	10.57	10.67
- hygroscopic		wt %	3.18	3.50	3.25	3.70
Volatile	V^{daf}	wt %	30.47	29.75	29.40	30.13

Table 6. Ultimate analysis of bituminous coal used in performance tests

Specification		Unit	Test #1	Test #2	Test #3	Test #4
Carbon	C^{ad}	wt %	63.76	61.30	61.82	62.29
Hydrogen	H^{ad}	wt %	3.39	3.20	3.55	3.39
Nitrogen	N^{ad}	wt %	1.03	1.02	1.03	1.01
Oxygen	O^{ad}	wt %	5.99	6.42	6.11	6.19
Sulphur	S^{ad}	wt %	1.42	1.12	1.19	1.24

The typical particle size distribution (PSD) of the materials supplied to the combustion chamber is shown in Fig. 3.

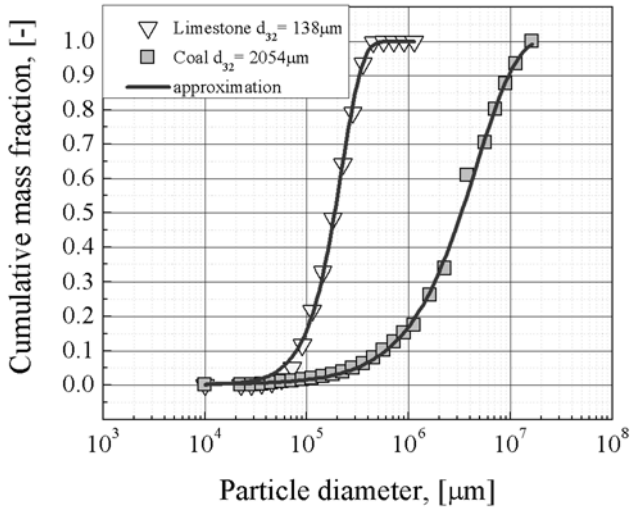

Fig. 3. Particle size distribution of the solids at supercritical CFB boiler

Moreover, Sauter mean diameters, d_{32}, are drawn in Fig. 3 for the solid materials (i.e. coal and limestone). The Sauter mean diameter of the solid materials, including fuel and limestone varied between 138 μm and 2054 μm. The Sauter mean particle diameter of the bed material, including sand, fuel, sorbent and ash, varied between 220 μm and 268 μm during the test performance in a 1294 t/h supercritical CFB boiler.

Table 7 shows the chemical composition of the sorbent utilised in the full-scale performance tests. One kind of limestone (Czatkowice limestone from Poland) was employed as a sorbent during the test run. Sorbent was also analysed by emission spectrometry for the content in the most important carbonates and other compounds. As expected, the main constituent of samples is $CaCO_3$ and in the limestone there is also a certain amount of $MgCO_3$. The calcium carbonate content ranged from 92.17 to 97.24 wt% and the magnesium carbonate content over the range 0.87-2.15 wt% was observed. The content of other species in the analysed limestone amounted to 4.10% on average.

Table 7. Chemical compositions of the limestone

Test run	Ca wt%	CaO wt%	$CaCO_3$ wt%	Mg wt%	MgO wt%	$MgCO_3$ wt%
#1	38.22	53.51	95.44	0.48	0.80	1.67
#2	36.91	51.67	92.17	0.62	1.03	2.15
#3	38.45	53.83	96.02	0.25	0.41	0.87
#4	38.94	54.51	97.24	0.29	0.48	1.01

5. RESULTS AND DISCUSSION

In this work, all measured results are given in the dimensionless scale and referred to the maximum value of furnace data inside the combustion chamber during all tests. The unit load variation in a supercritical CFB boiler determines the range of furnace temperature in the combustion chamber. The temperature distribution within the boiler's combustion chamber was in the range from 1033 K to 1153 K. Registered temperatures are in the range of typical temperatures for CFB boilers of 1023-1173 K, which is the best option from the thermal-flow conditions for gaseous emission reduction. Figure 4 shows the temperature distribution at different loads and relative height of furnace. It shows that

relative differential temperature inside the furnace chamber varied between 276.3 K and 287 K on average. The relative differential temperature was referred to the minimum value of bed temperature difference within the combustion chamber during all performance tests.

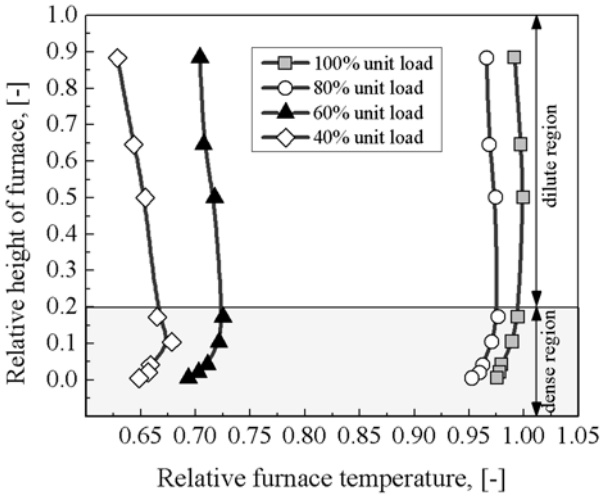

Fig. 4. Measured results of temperature profiles versus furnace height in the 1296 t/h supercritical CFB boiler

The highest relative temperature differences within the combustion chamber were at 40% MCR unit load. On the other hand, the lowest relative temperature difference was observed at 100% MCR unit load. On the basis of the furnace temperature data, it is evident that the temperature profiles in the furnace chamber have a nonlinear character, especially in the case of 40% unit load. The reason for this was an impact of the secondary air on the temperature distribution within the furnace chamber, where the fuel was burned out. As the combustion chamber height increases, the furnace temperature reaches the highest value at the middle of the furnace chamber and then gradually decreases in the upper part of the combustion chamber. When the supercritical CFB boiler was operating at 40% of the full load, the lowest temperature at the exit region of the furnace chamber was obtained. In the bottom part of the combustion chamber (i.e. dense region) significant temperature gradients existed, which ranged from 274.2K/m to 277K/m on average. In the dilute phase of solids suspension, the temperature gradient varied between 273.3K/m and 273.6K/m.

The variation of the furnace pressure with vertical distance from nozzles of the primary air is presented in Fig. 5.

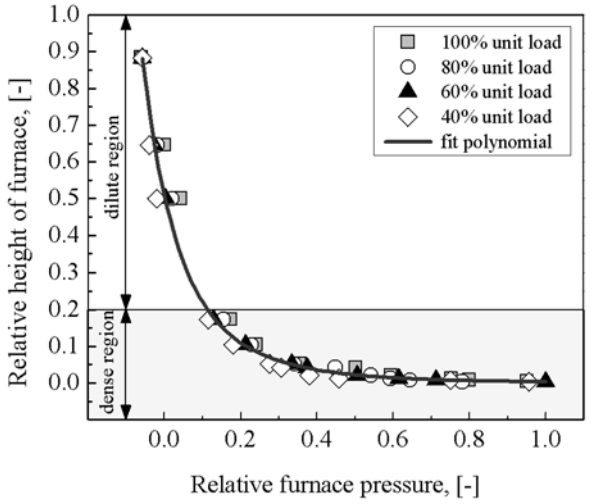

Fig. 5. Measured results of pressure profiles versus furnace height in the 1296 t/h supercritical CFB boiler

The furnace pressure decreased with an increase in the furnace height. It can be seen that the area of zero pressure was observed in the upper region of combustion chamber (i.e. dilute region).

When the 1296 t/h supercritical CFB boiler was operated at 100% and 80% unit load, the area of zero pressure was found at 31.2m distance from the grid. In the case of lower unit loads, the area of zero pressure was observed at 24 m up the grid. The highest pressure gradient inside the combustion chamber was recorded in the dense phase just above the grid (i.e. 527-798 Pa/m), and the lowest pressure gradient was measured in the upper part of the furnace occupied by a dilute phase (i.e. 15-44 Pa/m). Moreover, it can be seen that maximum pressure drop in the combustion chamber was kept at 8825 Pa. On the basis of these pressure data, the pressure distribution inside the combustion chamber remained in agreement with the typical pressure fluctuations for CFB boilers.

The empirical correlation of the overall heat transfer coefficients of water wall in the furnace chamber for large-scale CFB boilers is correlated with solid suspension density and furnace temperature using the following regression analysis:

$$h = K\left(\rho_b\right)^{\alpha}\left(T_b\right)^{\beta} \tag{10}$$

where values of K, α and β are the regression coefficients, fitted for certain ranges of the operating conditions. The solid suspension density, ρ_b, was determined by measuring the static pressure drop on the water wall. It is widely recognised that suspension density is strongly correlated with the height of the furnace chamber. During all test runs, suspension density in the dilute region (Fig. 6) was varied between 1.20 kg·m^{-3}and 6.31 kg·m^{-3}. On the other hand, the suspension density in the dense region (Fig. 6) ranged from 497 kg·m^{-3} to 553 kg·m^{-3}.

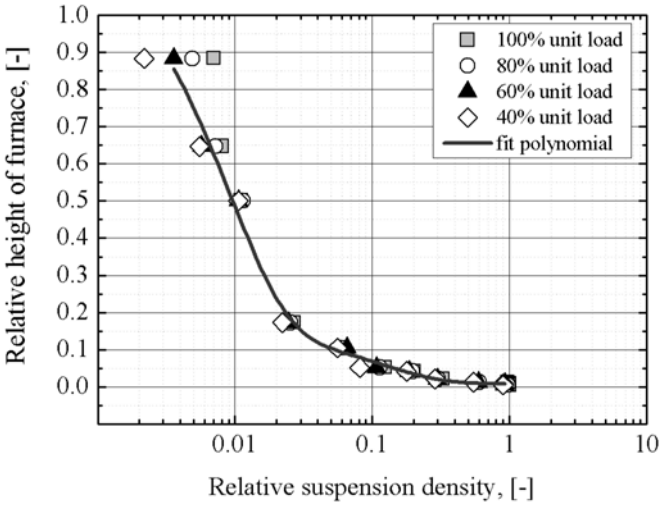

Fig. 6. Vertical solid suspension density profiles

A significant difference (ca. 461 times) in solid suspension density between the grid zone (i.e. dense region) and the upper part of the furnace (i.e. dilute region) was observed. The higher solid suspension density resulted from a higher concentration of particles in the bottom zone of the furnace. A very uniform density of gas – solids phase was found above 18 m distance from the grid at full load. In the lower region of the combustion chamber the bed material is characterised by high density and high turbulence coefficient. The existence of large pressure gradients in the bottom zone of the furnace chamber is a confirmation of this fact. The profiles shown in Fig. 6 are clearly very similar to the pressure profiles in the furnace seen in Fig. 5. The typical profiles of the suspension density are S-shaped, which is generally the case for CFB boilers. The shape of the suspension density profiles in Figure 6 resulted from distribution of the secondary air injection levels inside furnace chamber. They also depend upon the ratio of primary to secondary air. During performance tests, the parameter *PA/SA*

was greater at higher CFB unit load. Hence, the bed material from the dense lower section was transported to the upper part of the combustion chamber. Below the secondary air injection levels, there is an exponential decay of the suspension density. On the other hand, the solid suspension density profiles confirmed that above the secondary air injection levels solids transport occurs without a splash zone as the boundary between dense bed and dilute phase. Figure 7 shows a variation of the heat transfer coefficients at different unit loads and height of the combustion chamber. Figure 7 reveals that the convective heat transfer slightly increases as the boiler load increases. The data in the Fig. 7 do not indicate any significant influence of the unit load on the heat transfer coefficient. There is a certain scatter (max. ±19%) of the data, especially for the results obtained in the exit region of the furnace chamber.

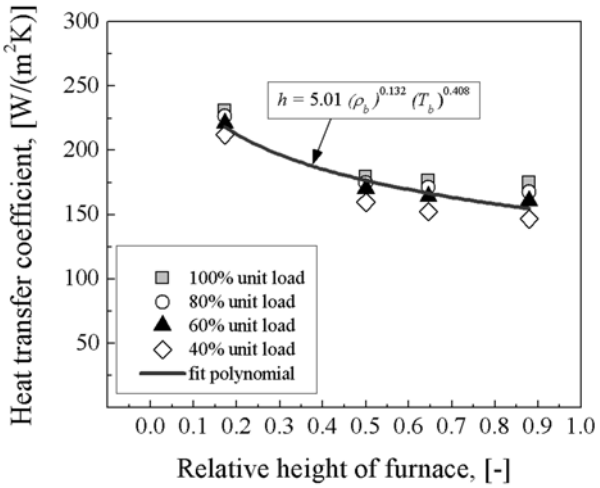

Fig. 7. Heat transfer coefficient versus furnace height in the 1296t/h supercritical CFB boiler

The main reason for this is that the heat transfer coefficient is dependent not only on solid suspension density, but also on the thermal boundary layer thickness and fluid mechanics. A thicker thermal boundary layer causes a reduction of the bed-to-wall heat transfer coefficient. This particular phenomenon could be observed in the region of diluted circulating bed material, where a weak mixing process of solid phase with gaseous phase occurred. Thus, in the case of the 1296 t/h supercritical CFB boiler a decrease of the heat transfer coefficient with increasing furnace height, due to dilute nature of the bed material (i.e. reduced cluster solids fraction) is counteracted by the smaller thickness of the thermal boundary layer. Moreover, solids circulation rate and separation efficiency affect suspension density in the exit region of the combustion chamber. During all test runs, separation efficiency was not lower than 99.84% and solids circulation rate, *KR*, ranged from 45 to 68 at 40% and 100% unit load, respectively. The solids circulation rate was determined on the basis of the fuel and limestone mass flows fed to the furnace chamber and the circulating material mass flow in the return system using the following Equation (11):

$$KR = \frac{\dot{m}_{\text{down}}}{\dot{m}_{\text{fuel}} + \dot{m}_{\text{sorbent}}} \tag{11}$$

where circulating material mass flow $\dot{m}_{down}$ is precisely explained in the work (Blaszczuk et al., 2013). Solid mass flows of coal and limestone were determined on the basis of 5-minute-interval-changes in the silos weight. Separation efficiency was calculated in agreement with following relationship (12):

$$\eta_{\text{cycl}} = 1 - \exp\left\{ -h \cdot \left(\frac{2\pi \cdot \left(U_0 \cdot R_{\text{cycl}}\right)^2 \cdot H_{\text{cycl}}}{\beta_{\text{drag}} \cdot R_{\text{nur}}^2 \cdot \dot{V}_g} - 1 \right) \right\} \tag{12}$$

where h denotes geometric coefficient for the cross-section solids separator whereas solids velocity is equal to zero, U_0 represents gas velocity inlet to solids separator in ms^{-1}, R_{cycl} is a separator diameter in m, H_{cycl} denotes separator height in m, β_{drag} represents a function determined in agreement with formula proposed by Bis (2010), R_{nur} is a vortex diameter in m and V_g denotes gas stream flow through solids separator in m^3h^{-1}. In the case of low solids circulation rate, drag force acting on the bed material particles predominates due to smaller number of solids particles in the exit region of the furnace chamber. Hence, a low solid concentration results in low heat transfer coefficient values. The relationship between the heat transfer coefficient and the circulated solids mass flux is less sensitive to the mean particle diameter than that for suspension density; probably because the mass flux itself is a function of particle diameter (Pagliuso et al., 2000; Tian and Peng, 2004). The circulated flux is directly proportional to the suspension density and inversely proportional to the particle diameter.

Figure 8 presents the bed-to-wall overall heat transfer coefficient variation with relative solid suspension density for different unit loads of the supercritical CFB boiler. The overall heat transfer coefficient significantly increases with increasing suspension density due to the following reasons. Firstly, the increase of suspension density is the result of higher cluster concentration in the vicinity of the water-wall. Also, due to higher solid suspension density, the gas-gap thickness decreases. Near the membrane water-wall, solids in the form of agglomerates or clusters flow downwards. There is a gas layer with only a few particles between the wall and the clusters, where particles will flow upwards in the center of furnace chamber. More details on cluster formation are reported by Reddy (2003) and (Nirmal Vijay and Reddy, 2005). The overall heat transfer coefficient in the 1296 t/h supercritical CFB unit depends on the solids concentration and bed hydrodynamic conditions. In dilute region the wall is covered by only a few clusters (ca. f = 17%) and is exposed mostly to dispersed phase, whereas under dense phase conditions the water-wall is covered by more clusters (ca. f = 49%).

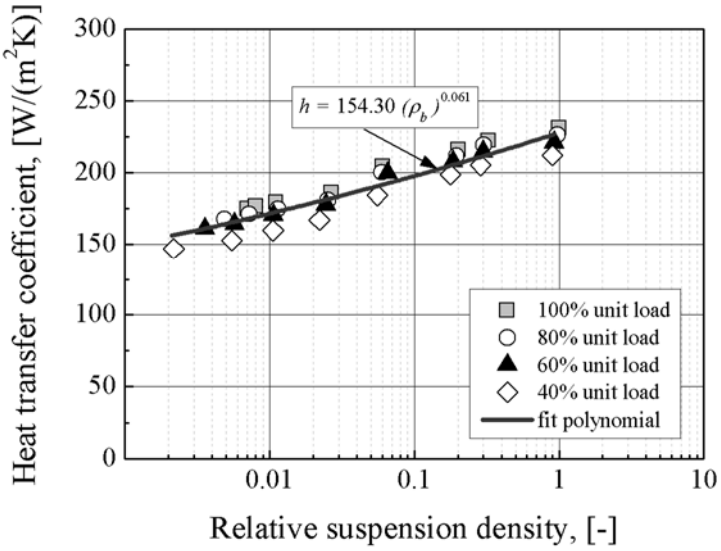

Fig. 8. Overall heat transfer coefficient versus relative solid suspension density in the 1296 t/h supercritical CFB boiler

6. CONCLUSIONS

It was possible to estimate heat transfer coefficient values inside the furnace chamber with the accuracy of ±19%. Equation (10) can be used to predict the bed-to-wall heat transfer coefficient and experimental investigation indicates the impact of operating parameters on the overall heat transfer coefficient. Empirical correlation of the heat transfer coefficient in a large-scale supercritical CFB boiler was mainly determined by the two key operating parameters, i.e. suspension density and bed temperature. The suspension density decreased along the furnace height and ranged from 1.20 $kg \cdot m^{-3}$ to 553 $kg \cdot m^{-3}$ during performed test runs. The temperature distribution within the boiler's combustion chamber was in the range from 1033K to 1153K. Registered temperatures are in the range of typical temperatures for CFB boilers of 1023-1173K. The bed-to-wall heat transfer coefficient was in the range of 146–231 $W/(m^2 \cdot K)$ in the 1296 t/h supercritical CFB boiler. At the exit region of furnace chamber, the heat transfer coefficient value ranged from 146 $W/(m^2 \cdot K)$ to 174 $W/(m^2 \cdot K)$. In the bottom region of combustion chamber the heat transfer coefficient had higher values (i.e. 212-231 $W/(m^2 \cdot K)$) because of higher solid suspension density. In the 1296 t/h supercritical CFB boiler the overall heat transfer coefficient depends on solid suspension density and bed hydrodynamic conditions in the direct vicinity of the membrane water-wall. Trend of variation was proportional to the fractional power of suspension density. These variation trends of the heat transfer coefficient are consistent with the available experimental data for large-scale CFB boilers. The present work provides some information about the heat transfer mechanism in the dilute/dense region of the furnace chamber, which are useful for scale-up and design of heat transfer surfaces for CFB boilers.

The authors would like to gratefully acknowledge the staff of Tauron Generation S.A. Lagisza Power Plant for technical support with supplying operating data.

SYMBOLS

c	specific heat, J/(kg·K)
e	emissivity
g	acceleration due to gravity, m/s^2
H	furnace height, m
H_i	furnace height at bottom level above grid in Equation (9), m
H_{i+1}	furnace height at upper level above grid in Equation (9), m
h	-to-wall heat transfer coefficient, $W/(m^2 \cdot K)$
K	regression coefficient in Equation (10)
k	thermal conductivity, W/(m·K)
U_{mf}	minimum fluidisation velocity, m/s
U_0	superficial gas velocity, m/s
U_t	terminal velocity, m/s
SA/PA	secondary air to primary air ratio
T_b	furnace temperature, K

Greek symbols

α	correlation constant in Equation (10)
β	correlation constant in Equation (10)
δ	non-dimensional gas layer thickness between the wall and cluster
Δp	pressure drop, kPa
ρ_b	suspension density, kg/m^3
σ	Stefan-Bolzmann constant

Superscripts

ad	air dried basis
ar	as received
daf	dry ash free

Subscripts

b	bed
c	clusters
g	gas
i	lower level above the grid
i+1	higher level above the grid
p	particle
w	wall

REFERENCES

Andersson B.-Å., 1996. Effects of bed particle size on heat transfer in circulating fluidized bed boilers. *Powder Technol.*, 87, 239-248. DOI: 10.1016/0032-5910(96)03092-6.

Basu P., Cheng L., 2000. An experimental and theoretical investigation into the heat transfer of a finned water tube in a circulating fluidized bed boiler. *Int. J. Energy Res.*, 24, 291-308. DOI: 10.1002/(SICI)1099-114X(20000325)24:4<291::AID-ER582>3.0.CO;2-I.

Basu P., 2006. *Combustion and gasification in fluidized beds*. Taylor & Francis Group, 193.

Bis Z., 2010. *Fluidized Bed Boilers. Theory and Practice*. Czestochowa University of Technology Press, Czestochowa, 215-227 (in Polish).

Blaszczuk A., Leszczynski J., Nowak W., 2013. Simulation model of the mass balance in a supercritical circulating fluidized bed combustor. *Powder Technol.*, 246, 313-326. DOI: 10.1016/j.powtec.2013.05.039.

Błaszczuk A., Komorowski M., Nowak W., 2012. Distribution of solids concentration and temperature within combustion chamber of SC-OTU CFB boiler. *J. Power Technol.*, 92, 27-33.

Breitholz C., Leckner B., Baskakov A.P., 2001. Wall average heat transfer in CFB boilers. *Powder Technol.*, 120, 41-48. DOI: 10.1016/S0032-5910(01)00345-X.

Cheng L., Wang Q., Shi z., Luo Z., Ni M., Cen K., 2007. Heat transfer in a large-scale circulating fluidized bed boiler. *Front. Energy Power Eng.*, 1 477-482. DOI: 10.1007/s11708-007-0071-5.

Dutta A., Basu P., 2002. Overall heat transfer to water walls and wing walls of commercial circulating fluidized bed boilers. *Journal of the Institute of Energy*, 75 (504), 85-90.

Dutta, A., Basu, P. 2004. An improved cluster-renewal model for the estimation of heat transfer coefficients on the furnace walls of commercial circulating fluidized bed boilers. *J. Heat Trans.*, 126, 1040-1043. DOI: 10.1115/1.1833360.

Feugier A., Gaulier C., Martin G., 1987. Some aspects of hydrodynamic, heat transfer and gas combustion in circulating fluidized beds. *Proceedings of the Eighth International Conference on Fluidized Bed Combustion*, Morgantown, USA, 613-618.

Goidich S.J., 2007. Supercritical boiler options to match fuel combustion characteristic. *Power-Gen Europe*, Madrid, 26-28 June 2007, 9-20.

Gorliz M.R., Grace J.R., 2002. Predicting heat transfer in large-scale CFB boilers, In: Grace J.R., Zhu J.X., de Lasa H (Eds.), *Circulating Fluidized Bed Technology VII*. Canadian Society for Chemical Engineering, Gilmore Printing Services Inc., 121-128.

Gungor A., 2009. A study on the effects of operational parameters on bed-to-wall heat transfer. *App. Therm. Eng.*, 29, 2280-2288. DOI: 10.1016/j.applthermaleng.2008.11.008.

Kobyłecki R., 2011. The possibility to co-fire lignite with hard coal and biomass – Operational experiences from a large-scale CFBC. *Rynek Energii*, 6, 151-155.

Koksal M., Gorliz M.R., Hamdullahpur F., 2008. Effect of staged air on heat transfer in circulating fluidized beds. *App. Therm. Eng.*, 28, 1008-1014. DOI: 10.1016/j.applthermaleng.2007.06.028.

Lints M.C., Glicksman L.R. 1994. Parameters governing particle to wall heat transfer in a circulating fluidized bed, In: Avidan A.A. (Ed.), *Circulating Fluidized Bed Technology - IV*. AIChE, New York, 297-304.

Nirmal Vijay G., Reddy B.V., 2005. Effect of dilute and dense phase operating conditions on bed-to-wall heat transfer mechanism in a circulating fluidized bed combustor. *Int. J. Heat Mass Tran.*, 48, 3275-3283. DOI: 10.1016/j.ijheatmasstransfer.2005.03.013.

Noymer, P.D., Glicksman, L.R. 2000. Descent velocities of particle clusters at the wall of a circulating fluidized bed. *Chem. Eng. Sci.*, 55, 5283-5289. DOI: 10.1016/S0009-2509(00)00171-8.

Pagliuso J.D., Lombardi G., Goldstein Jr. L., 2000. Experiments on the local heat transfer characteristics of circulating fluidized bed. *Exp. Therm. Fluid Sci.*, 20, 170-179. DOI: 10.1016/S0894-1777(99)00042-4.

Reddy B.V., 2003. Fundamental heat transfer mechanism between bed –to membrane water-walls in circulating fluidized bed combustors. *Int. J. Energy Res.*, 27, 813-824. DOI: 10.1002/er.911.

Shi D., Nicolai R., Reh L., 1998. Wall-to-bed heat transfer in circulating fluidized bed boilers. *Chem. Eng. Process.*, 37, 287-293. DOI: 10.1016/S0255-2701(98)00039-7.

Tian Y., Peng X.F., 2004. Analysis of particle motion and heat transfer in circulating fluidized beds. *Int. J. Energy Research*, 28, 287-297. DOI: 10.1002/er.965.

Werther J., 2005. Fluid dynamics, temperature and concentration fields in large-scale CFB combustors, In: Cen K. (Ed.), *Circulating Fluidized Bed Technology – VIII*. International Academic Publishers, Beijing, 10-13 May 2005, 1-25.

Wu R.L., Lim C.J., Grace J.R., Brereton C.M.H., 1991. Instantaneous local heat transfer and hydrodynamics in a circulating fluidized bed. *Int. J. Heat Mass Trans.*, 34, 2019-2027. DOI: 10.1016/0017-9310(91)90213-X.

Xie D., Bowen B.D., Grace J.R., Lim C.J., 2003. Two-dimensional model of heat transfer in circulating fluidized beds. Part II: Heat transfer in a high density CFB and sensitivity analysis. *Int. J. Heat Mass Tran.*, 46, 2193-2205. DOI: 10.1016/S0017-9310(02)00528-8.

Zhang H., Lu J.F., Yang H.R., 2005. Heat transfer measurements inside the furnace 135MWe CFB boiler, In: Cen Kefa (Ed.), *Circulating Fluidized Bed Technology VIII*. International Academic Publishers, World Publishing Corporation, 254-260.

Received 04 March 2013
Received in revised form 29 January 2014
Accepted 13 March 2014